Transition Metal Chemistry
https://doi.org/10.1007/s11243-018-0244-2

A manganese Schiff base complex immobilized on copper–ferrite magnetic nanoparticles as an efficient and recyclable nanocatalyst for selective oxidation of alcohols

Mahmood Tavakoli Hafshejani[1] · **Samira Saeednia**[1] · **Mehdi Hatefi Ardakani**[1] · **Zahra Pakdin Parizi**[2]

Received: 18 February 2018 / Accepted: 2 May 2018

Abstract

A magnetically recoverable nanocatalyst was synthesized by covalent binding of a Schiff base ligand, namely *N*,*N*′-bis(Salicylidene)-1,3-diaminopropane-2-ol (H_2salpn), onto the surface of silica-coated magnetic $CuFe_2O_4$ nanoparticles, followed by complexation with $MnCl_2$. The resulting core–shell nanoparticles were characterized by spectroscopic and microscopic methods, including FTIR, XRD, VSM, TGA elemental analysis, TEM, and SEM. The Mn content was determined by ICP analysis. The nanoparticles were investigated as a catalyst for the selective oxidation of alcohols to the corresponding carbonyl compounds with tertiary-butyl hydrogen peroxide. The catalyst can be magnetically separated for reuse, with no noticeable loss of activity in subsequent reaction cycles. FTIR, VSM, and leaching experiments after three successive cycles confirmed that the catalyst was strongly anchored to the magnetic nanoparticles. A suitable mechanism for the reaction is proposed.

Introduction

Oxidation reactions are among the most useful processes in organic synthesis, since the products of these reactions are widely used as intermediates in the pharmaceutical and fine chemical industries [1, 2]. Among the various kinds of oxidations, the oxidation of alcohols to carbonyl compounds is an essential transformation in the laboratory as well as industry [3, 4]. Traditional oxidation methods are associated with heavy metals, toxic and environmentally polluting reagents, high temperatures, and moderate chemoselectivities. Therefore, much research has been focused on the development of economical and environmentally benign oxidation processes [5–7].

Oxidation reactions are generally carried out in homogeneous systems. Although homogeneous catalysts often show higher catalytic activities than their heterogeneous counterparts, they can also suffer from difficulties of separation and recovery of the catalyst from both the reaction mixture and the products [8–13]. Therefore, the immobilization of homogeneous catalysts on solid supports has attracted substantial interest. Recently, various supports have been used for the immobilization of homogeneous catalysts, including mesoporous silica [14–18], polymers [19, 20], activated carbon [21, 22], and inorganic nanoporous materials [23]. Magnetic nanoparticles have attracted considerable attention due to their unique properties. They have been used in various fields such as magnetically assisted drug delivery, magnetic resonance imaging, contrast agents and hyperthermia treatments [24–29]. One of the most frequent applications of magnetic nanoparticles is as a substrate for catalysts [30, 31].

Ferrites are a class of magnetic nanoparticles which have found various applications as image contrast agents [32], bioseparation sensors [33, 34], and biomedicines [35, 36]. There have been widespread studies on the synthesis of magnetic core–shell nanostructures because of their particular magnetic properties [37–39]. Coating a silica shell around magnetic nanoparticles provides several advantages, such as improving the dispersion and enhancement of catalytic

---

Electronic supplementary material The online version of this article (https://doi.org/10.1007/s11243-018-0244-2) contains supplementary material, which is available to authorized users.

✉ Samira Saeednia
sami_saeednia@yahoo.com; s.saeednia@vru.ac.ir

[1] Department of Chemistry, Faculty of Science, Vali-e-Asr University of Rafsanjan, Rafsanjan 77188-97111, Iran

[2] Department of Nuclear Medicine and Molecular Imaging, Razavi Hospital, Mashhad 9198613676, Iran

activity [40]. The silica layer can also protect the core from corrosion during oxidation and epoxidation reactions [41].

The immobilization of manganese complexes on solid supports has already received much attention. Manganese complexes are often easily synthesized, with mild reaction conditions and short reaction times [42–46]. Given that ferrites require an inert atmosphere for synthesis [42, 43], in this study copper–ferrite was used as a magnetic core. The magnetism of this material is almost the same as that of ferrites, but the preparation is easier, with no need for an inert atmosphere. To the best of our knowledge, this is the first report on the synthesis of a Mn Schiff base complex immobilized on copper–ferrite nanoparticles as a magnetic core.

This report describes a simple and efficient synthesis of a copper–ferrite supported magnetically recyclable and inexpensive manganese Schiff base catalyst and its application for the oxidation of alcohols to the corresponding carbonyl compounds using tertiary-butyl hydrogen peroxide (TBHP) in ethanol. The catalyst can be easily and completely separated from the reaction mixture by the application of an external magnetic field.

Experimental

Chemicals were purchased from Merck or Fluka and used without further purification. The purities of the reaction products and the overall progress of the reactions were checked by TLC on silica gel polygram SILG/UV254 plates. TEM analysis was performed with a TEM microscope (Philips CM30). FTIR spectra were recorded in the 4000–400 cm^{-1} region, using KBr disks, on a Thermo SCIENTIFIC model NICOLET iS10 spectrophotometer. Elemental analyses were obtained on a LECO CHNS-932 analyzer. Thermogravimetric analysis (TGA) was performed on a computer-controlled Rheometric Scientific model STA 1500 instrument. Powder X-ray diffraction (XRD) was performed on a Philips X'pert diffractometer with Cu K_α ($\lambda = 0.154$ nm) radiation. Room-temperature magnetization isotherms were obtained using a vibrating sample magnetometer (VSM, LakeShore 7400). The Mn content in the catalyst was determined with an ICP-OES Optima DV7300 inductively coupled plasma analyzer. Gas chromatography experiments were performed with a Shimadzu 16A chromatograph using a column packed with silicon DC-200 and a flame ionization detector (FID).

Preparation of $CuFe_2O_4$ nanoparticles

$CuFe_2O_4$ nanoparticles were prepared by thermal decomposition of copper and iron salts in water in the presence of NaOH [44]. In a generic experiment, a solution of NaOH (3 g) in deionized water (15 mL) was added to a solution of $Fe(NO_3)_3 \cdot 9H_2O$ (3.34 g, 8.2 mmol) and $Cu(NO_3)_2 \cdot 3H_2O$ (1 g, 4.1 mmol) in deionized water (15 mL) at room temperature over 10 min. After forming a reddish-brown precipitate, the mixture was warmed to 90 °C and stirred under ultrasonic irradiation for 2 h and then cooled to room

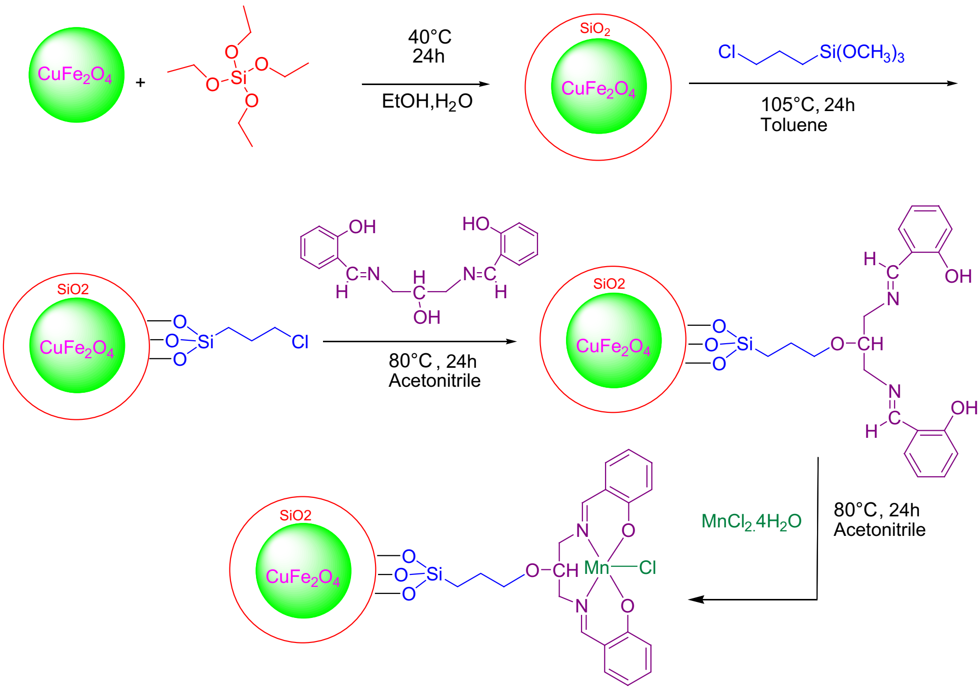

Scheme 1 Synthesis of $CuFe_2O_4@SiO_2$–MnClsalpn

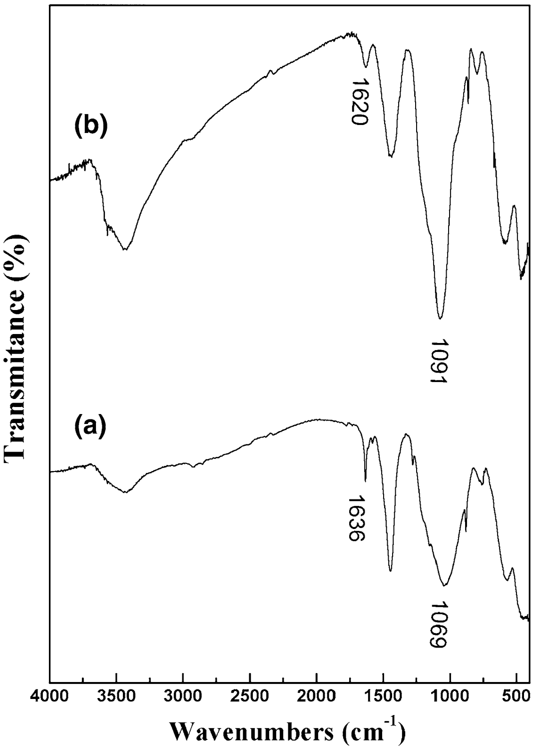

Fig. 1 FTIR spectra of (a) $CuFe_2O_4@SiO_2$–salpnH$_2$ and (b) $CuFe_2O_4@SiO_2$–MnClsalpn

temperature. The resulting particles were separated by an external magnet, then washed three times with deionized water, and dried under vacuum at 80 °C for 12 h. The nanoparticles were then ground in an agate mortar and kept in a furnace at 400 °C for 5 h and then cooled to room temperature. $CuFe_2O_4$ particles of about 45–55 nm diameters were so obtained.

Preparation of silica-coated magnetite ($CuFe_2O_4@SiO_2$ core–shell)

Concentrated aqueous ammonia (3.5 mL) was added slowly to a sonicated mixture of $CuFe_2O_4$ nanoparticles (3.5 g) suspended in deionized water–ethanol (40:160 mL), and the resulted mixture was stirred at 40 °C for 30 min. Tetraethyl orthosilicate (TEOS, 2.0 mL) was then added, and the mixture was stirred at 40 °C for 24 h. The silica-coated copper–ferrite magnetic nanoparticles ($CuFe_2O_4@SiO_2$) were isolated with a magnet. The collected solid was washed several times with EtOH and diethyl ether and then dried at 100 °C in a vacuum oven for 24 h [45].

Synthesis of chloro-functionalized $CuFe_2O_4@SiO_2$

$CuFe_2O_4@SiO_2$ (3.5 g) was sonicated in dry toluene (50 mL) for 30 min. 3-Chloropropyltriethoxysilane (3.5 mL) was

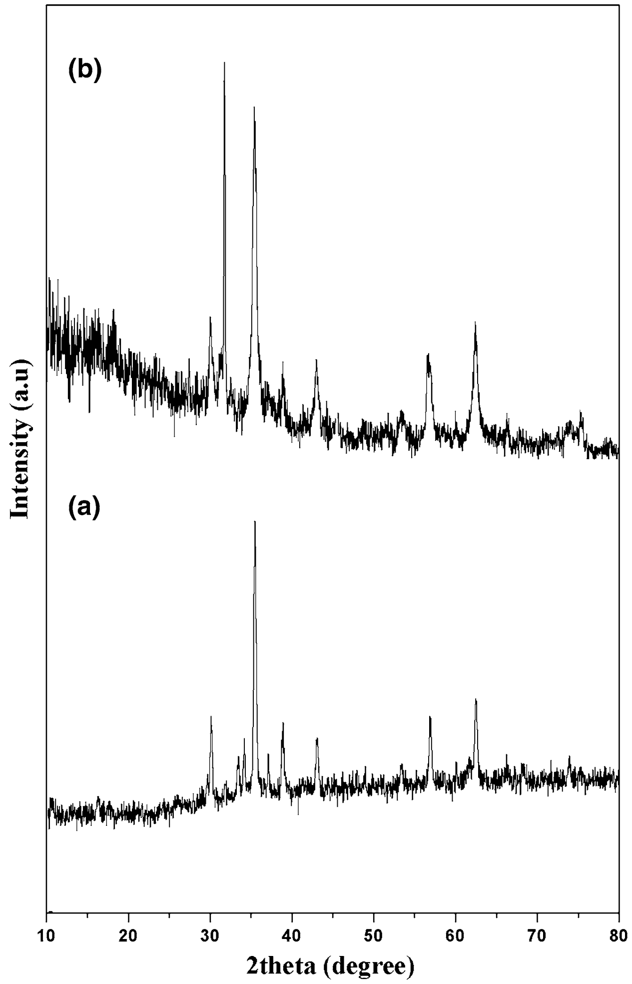

Fig. 2 XRD patterns of (a) $CuFe_2O_4$ and (b) $CuFe_2O_4@SiO_2$–MnClsalpn

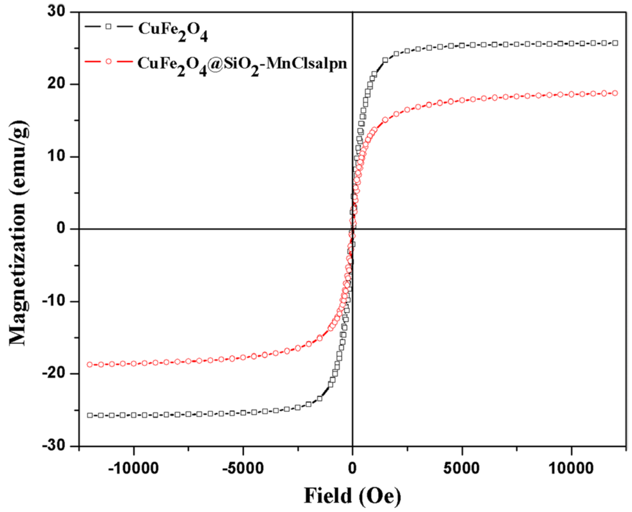

Fig. 3 Magnetization curves of (a) $CuFe_2O_4$ and (b) $CuFe_2O_4@SiO_2$–MnClsalpn

then added to the suspension, and the mixture was stirred at 105 °C for 24 h. The solid was separated with an external magnet, washed several times with ethanol, and dried under vacuum [46].

Synthesis of supported Schiff base ($CuFe_2O_4@SiO_2$–salpnH$_2$)

SalpnH$_2$ (*N*,*N*′-bis(Salicylidene)-1,3-diaminopropane-2-ol) was prepared according to the reported method [47]. A portion of salpnH$_2$ (1 g, 3.2 mmol) was added to a sonicated suspension of $CuFe_2O_4@SiO_2$ (2 g) in acetonitrile (100 mL), and the resulting mixture was refluxed for 24 h. The solid was separated magnetically, washed thoroughly with ethanol, and dried under vacuum.

Synthesis of $MnCl_2$ salpn-modified $CuFe_2O_4@SiO_2$ ($CuFe_2O_4@SiO_2$–MnClsalpn)

$CuFe_2O_4@SiO_2$–salpnH$_2$ (2.5 g) was sonicated in dry acetonitrile (100 mL) for 30 min. To the resulting suspension, $MnCl_2.4H_2O$ (2 g) was added, and the mixture was refluxed for 24 h. The solid was separated with an external magnet and was subjected to Soxhlet extraction with ethanol and then dried under vacuum at 90 °C for 12 h to give $CuFe_2O_4@SiO_2$–MnClsalpn.

General procedure for oxidation of alcohols

All catalytic experiments were performed in a 5-mL test tube. In a typical procedure, to a solution of benzyl alcohol (1 mmol) in solvent (0.5 mL), $CuFe_2O_4@SiO_2$–MnClsalpn (0.0014 g, 2 mol %) and TBHP (2 mmol) were added. The reaction mixture was stirred for 1 h at 80 °C, and the products were tracked by TLC or GC. After completion of the reaction, the mixture was diluted with EtOAc. The catalyst was separated with an external magnet, washed with EtOAc, dried, and reused for a sequential run under the same reaction conditions. Evaporation of the solvent from the filtrate gave the crude product, which was purified by chromatography on silica gel with *n*-hexane/EtOAc (2:5).

Results and discussion

Scheme 1 shows the chemistry employed for the functionalization of $CuFe_2O_4$ magnetic nanoparticles (MNPs) with the manganese Schiff base complex. In the first step, the MNPs were coated with a silica shell to obtain $CuFe_2O_4@SiO_2$ core–shell. This outer shell of silica serves to improve the dispersibility of the nanoparticles and also provides surface Si–OH groups for further surface functionalization. Hence, the treatment of the silanol groups of $CuFe_2O_4@SiO_2$ with chloropropyl trimethoxysilane gives chloropropylated magnetite nanoparticles. In the next step, the chloro-functionalized $CuFe_2O_4@SiO_2$ was substituted by the alkoxide groups of salpnH$_2$ Schiff base to yield the $CuFe_2O_4@SiO_2$–salpnH$_2$, a tetradentate Schiff base ligand supported on $CuFe_2O_4@SiO_2$. Finally, the reaction of excess $MnCl_2\cdot4H_2O$ with $CuFe_2O_4@SiO_2$–salpnH$_2$ in dry acetonitrile gave $CuFe_2O_4@SiO_2$–MnClsalpn. The final product was subjected to Soxhlet extraction in order to remove unreacted $MnCl_2$.

Characterization of the nanoparticles

In order to confirm the modification of the magnetite surface, FTIR spectra of the prepared $CuFe_2O_4@SiO_2$–salpnH$_2$ and $CuFe_2O_4@SiO_2$–MnClsalpn materials were recorded, as shown in Fig. 1. The observation of two broad bands at around 466–581 cm^{-1} indicates the presence of the magnetite core in both samples. The silica coating of magnetite nanoparticles was confirmed by observation of a broad band

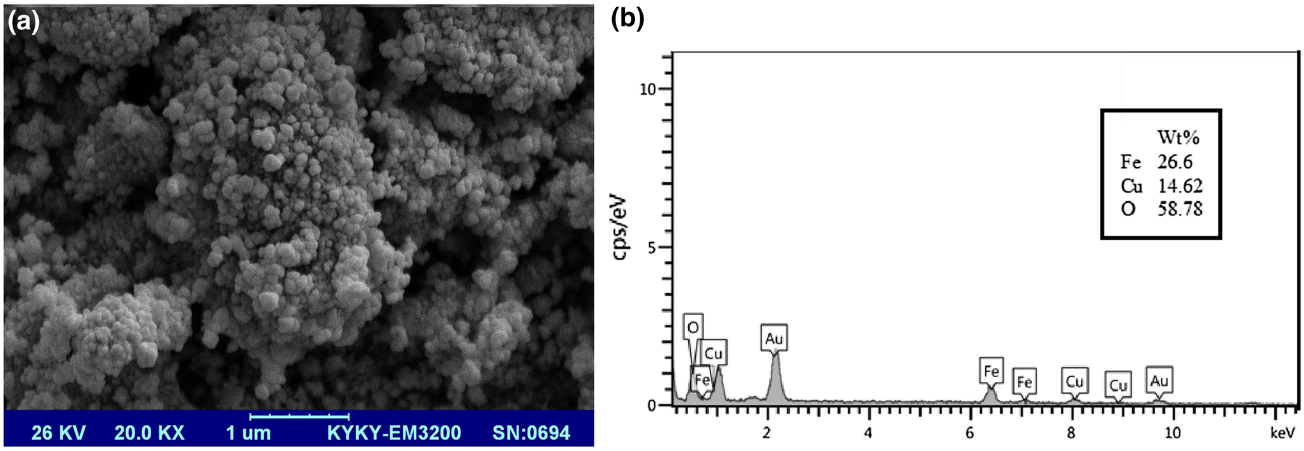

Fig. 4 **a** SEM image of $CuFe_2O_4$ and **b** EDAX analysis of $CuFe_2O_4$

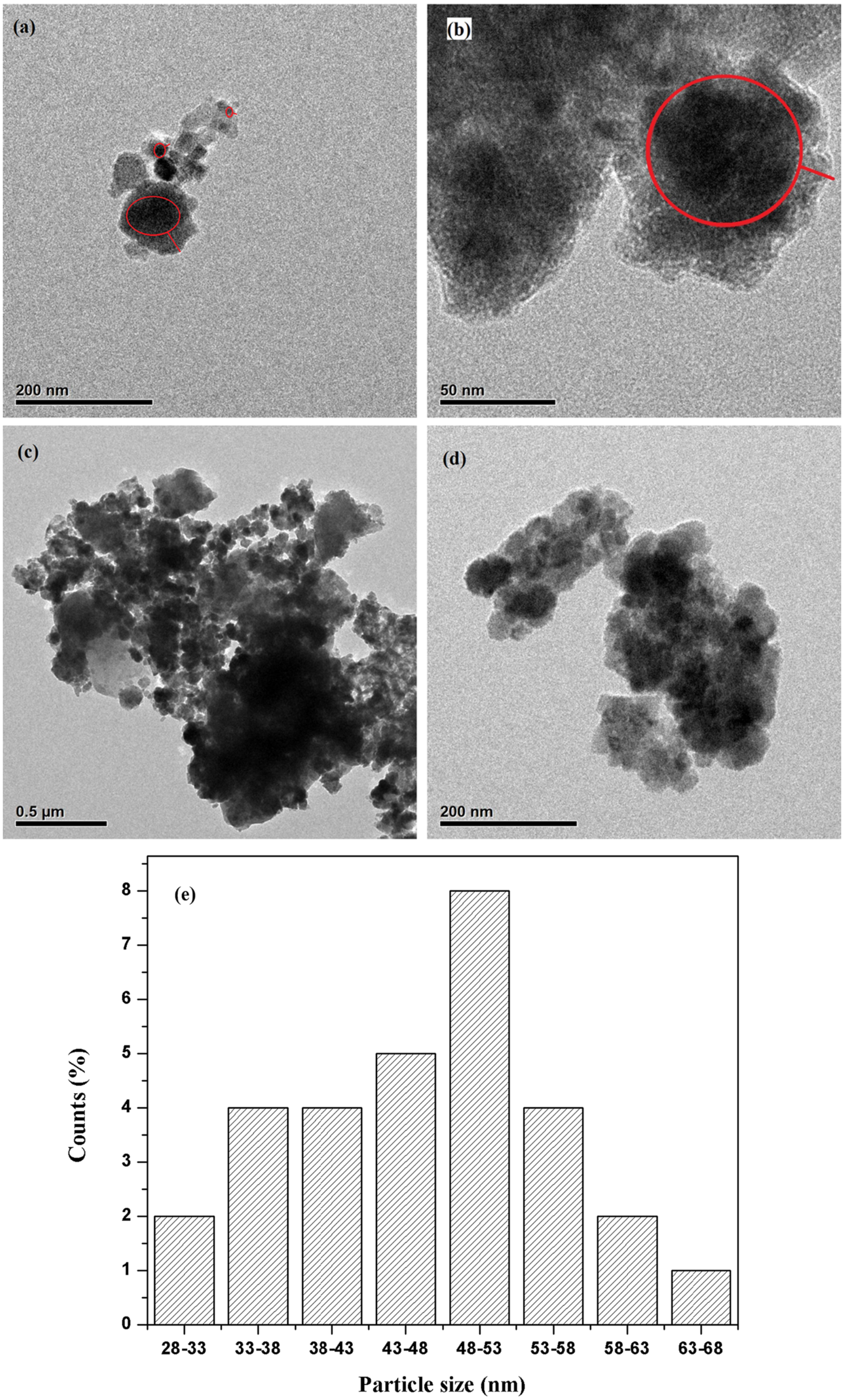

Fig. 5 **a**–**d** HRTEM images of $CuFe_2O_4@SiO_2$–MnClsalpn core–shell nanoparticles and **e** the particle size distribution of $CuFe_2O_4@SiO_2$–MnClsalpn

at about 1000–1100 cm^{-1} assigned to Si–O–Si and Si–OH stretching vibrations. In the FTIR spectrum of $CuFe_2O_4@SiO_2$–salpnH_2 (Fig. 1a), a band at 1636 cm^{-1}, assigned to the C=N stretching vibration of salpnH_2 [48, 49], and some weak bands at 1400–1500 cm^{-1} assigned to the aromatic rings of salpnH_2 were observed; these were not present in the parent $CuFe_2O_4@SiO_2$. Upon reaction with $MnCl_2$, the C=N band at 1636 cm^{-1} shifted to lower frequency (1620 cm^{-1}) (Fig. 1b), indicating complexation of the C=N groups to manganese. Further evidence for formation of $CuFe_2O_4@SiO_2$–MnClsalpn was also provided by the observation of

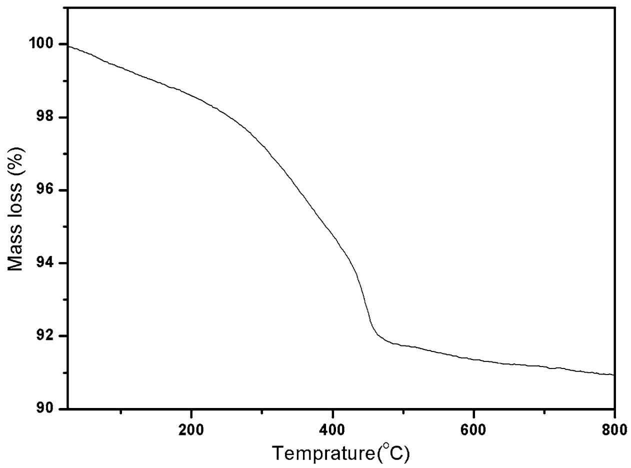

Fig. 6 TGA curve for $CuFe_2O_4@SiO_2$–MnClsalpn

Table 1 Oxidation of benzyl alcohol to benzaldehyde under different conditions

Entry	Oxidants	*T* (°C)	Solvent (0.5 ml)	Yield[a] (%)
1	TBHP	80	–	65
2	TBHP	80	EtOH	90
3	TBHP	80	Toluene	85
4	TBHP	65	CH_3OH	80
5	TBHP	55	THF	60
6	TBHP	60	$CHCl_3$	60
7	TBHP	80	CH_3CN	90
8	TBHP	60	CH_2Cl_2	20
9	TBHP	80	H_2O	60
10	TBHP	80	DMSO	20
11	TBHP	50	EtOH	50
12	O_2[b]	80	EtOH (1 ml)	40
13	H_2O_2	80	EtOH	Trace
14	UHP	80	EtOH	30
15	–	80	EtOH	Trace
16[c]	TBHP	80	EtOH	60
17[d]	TBHP	80	EtOH	50
18[e]	TBHP	80	EtOH	85
19[f]	TBHP	80	EtOH	Trace
20[g]	TBHP	80	EtOH	10
21[h]	TBHP	80	EtOH	30
22[i] (1st)	TBHP	80	EtOH	90
23[i] (2nd)	TBHP	80	EtOH	88
24[i] (3rd)	TBHP	80	EtOH	85

[a] Isolated yield, reaction conditions: benzyl alcohol (1 mmol), oxidant (2 mmol, except for entries 12–16), $CuFe_2O_4@SiO_2$–MnClsalpn (2 mol%, except for entries 17–21), reaction time: 1 h

[b] 60 bubble/min

[c] 1 mmol TBHP

[d] Catalyst: 1 mol%

[e] Catalyst: 3 mol%

[f] No catalyst

[g] Catalyst: $CuFe_2O_4$(2 mol%)

[h] Catalyst: $MnCl_2.4H_2O$ (2 mol%)

[i] Catalytic test with first, second and third recovered catalyst

ν(Mn–O) and ν(Mn–N) bands at ca. 570 and ca. 410 cm^{-1}, respectively [50, 51].

Figure 2 depicts the XRD pattern of the MNPs. The diffraction peaks can be assigned to the planes of inverse cubic spinel-structured $CuFe_2O_4$ (JCPDS no. 034-0425). The same confirming characteristic peaks were observed in the XRD pattern of $CuFe_2O_4@SiO_2$–MnClsalpn, confirming the stability of the crystalline phase during surface modification of the nanoparticles. The XRD pattern of $CuFe_2O_4@SiO_2$–MnClsalpn shows an obvious peak at $2\theta = 5–20$, assigned to amorphous silica (Fig. 2b). The broadening of each peak indicates the nanocrystalline nature of the as-prepared $CuFe_2O_4@SiO_2$–MnClsalpn. The average size of $CuFe_2O_4@SiO_2$–MnClsalpn deduced from Scherrer's formula was 36.4 nm.

In order to characterize the magnetic properties of the magnetite nanoparticles before and after surface modification, we recorded their hysteresis loops at room temperature using vibrating sample magnetometry (VSM). The magnetization curves are shown in Fig. 3. The MNPs exhibited no remaining effects (superparamagnetic properties) with saturation magnetization of about 25 emu/g. The surface-modified nanoparticles also showed superparamagnetic behavior, with decreased saturation magnetization of about 7 emu/g. The $CuFe_2O_4@SiO_2$–MnClsalpn nanoparticles showed a saturation magnetization of about 18 emu/g, sufficient for them to be separated easily and rapidly from the reaction mixture by use of an external magnet. Also, the superparamagnetic properties of the $CuFe_2O_4@SiO_2$–MnClsalpn nanoparticles are suitable to prevent aggregation and enable them to redisperse quickly when the magnetic field is removed.

A SEM micrograph of the synthesized $CuFe_2O_4$ nanoparticles is shown in Fig. 4. It is evident that the particles have almost uniform spherical morphology with a narrow size distribution. The size of the nanoparticles calculated from the SEM micrographs was in the range of 45–55 nm, which is in good agreement with the value obtained from the XRD data (the average size from Scherrer's formula was about 48.5 nm). The obtained EDAX spectrum (Fig. 4b) confirms the presence of Cu, Fe and O in the sample, with a Cu/Fe stoichiometry of 1:1.82 (semiquantitative analysis).

The effect of surface modification on the size and structure of the MNPs was evaluated by high-resolution transmission electron microscopy (HRTEM), which showed a spherical shape for $CuFe_2O_4@SiO_2$–MnClsalpn with diameter of ca. 50 nm (Fig. 5). It also confirmed the core–shell structure

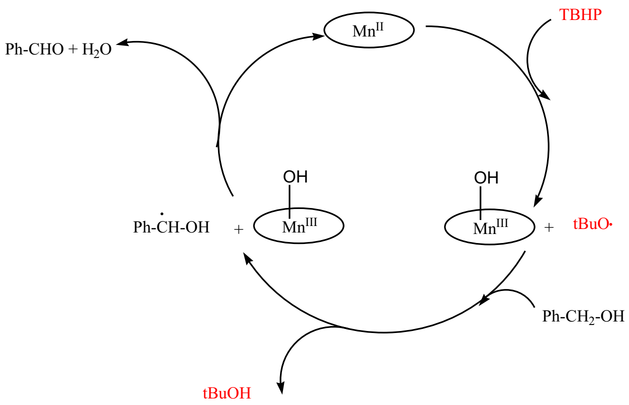

Scheme 2 Proposed mechanism for oxidation of benzyl alcohol with TBHP catalyzed by $CuFe_2O_4$@SiO_2–MnClsalpn

of the particles and confirmed the presence of a silica shell of uniform thickness (Fig. 5).

Thermogravimetric analysis (TGA) was used to investigate the thermal stability of $CuFe_2O_4$@SiO_2–MnClsalpn, as shown in Fig. 6. A weight loss of about 9 wt% between 25 and 600 °C can be attributed to decomposition of the organic component attached to the surface. According to the TGA, the amount of organic component functionalized on $CuFe_2O_4$@SiO_2 was about 9 wt%.

These results are in good agreement with the elemental analysis ($N = 0.53\%$) and the ICP analysis, which showed that 0.19 mmol of manganese was anchored on 1.0 g of $CuFe_2O_4$@SiO_2–MnClsalpn nanoparticles.

Catalytic oxidation of alcohols

The catalytic activity of $CuFe_2O_4$@SiO_2–MnClsalpn for the oxidation of alcohols to the corresponding aldehydes or ketones has been investigated. The oxidation of benzyl alcohol to benzaldehyde was chosen as a test reaction, with TBHP as the terminal oxidant. Our initial experiments focused on the choice of reaction solvent (Table 1, entries 1–10). The reaction was also investigated under solvent-free conditions. The best product yields were obtained in ethanol and acetonitrile at 80 °C (entries 2 and 7). Since ethanol is cheaper and less toxic, it was chosen as solvent for subsequent experiments. On lowering the temperature, the product yield was decreased (entry 11). Next, the influence of different oxidants on the oxidation of benzyl alcohol in ethanol at 80 °C was investigated (entries 12–14). TBHP proved to be the best option (entry 2). The reaction gave only a trace amount of the desired product in the absence of any added oxidant (entry 15). A similar reaction with 1 mmol of the oxidant gave a low yield (entry 16). Next, the influence of different amounts of $CuFe_2O_4$@SiO_2–MnClsalpn was studied. Entries 2, 17, and 18 show that 2 mol% of the catalyst gave the best results. The model reaction was also carried out in the absence of the catalyst, in the presence of $CuFe_2O_4$ and $MnCl_2.4H_2O$ rather than $CuFe_2O_4$@SiO_2–MnClsalpn (entries 19–21); under these conditions, the amount of the desired product was significantly decreased.

Metal-catalyzed oxidations by alkyl peroxides may proceed through homolytic or heterolytic mechanisms. Transition metal complexes of Co, Cu, Fe, and Mn are usually involved in hemolytic mechanisms [52–54]. Hence, an oxidation mechanism for benzyl alcohol by TBHP in the presence of $CuFe_2O_4$@SiO_2–MnClsalpn can be proposed as shown in Scheme 2.

In order to test the generality of this method, the oxidations of several primary and secondary alcohols under the optimized reaction conditions were investigated (Table 2). Substituted benzyl alcohols bearing either electron-releasing or withdrawing groups were also oxidized selectively, affording the corresponding aldehydes in good-to-excellent yields (entries 1–6). Moderately sterically hindered benzyl alcohols were also transformed to the corresponding aldehydes in good yields, without any over-oxidation to the corresponding carboxylic acid (entries 2, 3, 5). In particular, the heteroaromatic furfuryl alcohol, which is known to be a challenging substrate in most transition metal catalyst systems, was oxidized selectively to furfural in this system (entry 7). Meanwhile, secondary alcohols gave the corresponding ketones in good yields (entries 8–14).

The chemoselectivity of this system was investigated by means of a competitive reaction system. A mixture of equal amounts of benzyl alcohol and 2-phenyl ethanol was oxidized under the conditions given in Table 2 (Scheme 3). In this experiment, benzyl alcohol was quantitatively oxidized to benzaldehyde, while the 2-phenyl ethanol remained unreacted. In the absence of catalyst, only trace amounts of both oxidation products were obtained.

In order to show that nanocatalyst is truly heterogeneous, a hot filtration test was performed. In this experiment, benzyl alcohol was oxidized for 30 min (ca. 60% yield, Table 1). The nanocatalyst was then recovered magnetically at the reaction temperature to avoid re-adsorption of the solubilized species, and the solution was decanted into a clean test tube. The decantate was heated at 80 °C for 24 h to elucidate whether oxidation resulted from a homogeneous catalyst leached from the support, or from the surface-bound manganese catalyst. The yields were determined after 1 and 24 h, and it was found that the product amount increased only slightly and then remained constant (Table 1). When $CuFe_2O_4$@SiO_2–MnClsalpn was employed as catalyst, ICP analyses showed that only a very small amount of Mn (less than 2%) had been lost after the first run. The recyclability of a heterogeneous catalyst provides a critical advantage

Table 2 Oxidation of alcohols with TBHP catalyzed by $CuFe_2O_4@SiO_2$–MnClsalpn

Entry	Alcohol	Product [a]	Time(h)	Yield [b](%)	TON
1	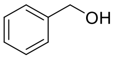	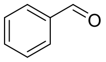	1	90	1691
2	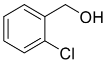	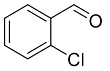	1	90	1691
3	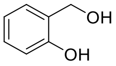	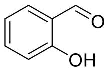	1	80	1503
4	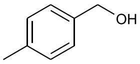	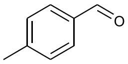	1	90 [c]	1691
5	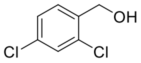	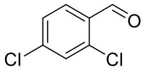	1	85	1597
6	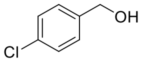	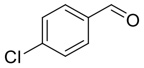	1	90 [d]	1691
7	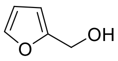	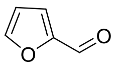	1	80	1503
8	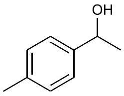	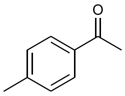	1	75	1409
9[e]	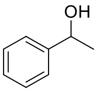	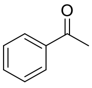	4	60	1127
10[e]	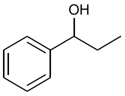	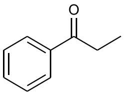	4	55	1034
11[e]	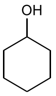	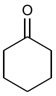	4	70	1315

Table 2 (continued)

Entry	Alcohol	Product [a]	Time(h)	Yield [b](%)	TON
12[f]	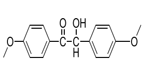	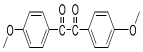	2	70	1315
13[f]	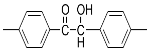	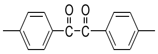	2	70	1315
14[f]	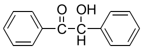	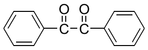	2	75	1410

Reaction conditions: alcohol (1 mmol), TBHP (2 mmol), catalyst (2 mol %), temperature: 80° C

[a] All products are identified by comparison of their physical data with those of authentic samples

[b] Isolated yield. Yields are determined by TLC and GC based on the starting alcohol

[c] ^{1}H NMR (500 MHz, $CDCl_3$) *δ*: 2.31 (*s*, 3H, CH3), 7.20 (*d*, *J* = 15 Hz, 2H, ArH), 7.66 (*d*, *J* = 15 Hz, 2H, ArH), 9.95 (*s*, 1H, aldehyde H)

[d] ^{1}H NMR (500 MHz, $CDCl_3$) *δ*: 7.26–7.82 (*m*, 4H, ArH), 9.96 (*s*, 1H, aldehyde H)

[e] TBHP (4 mmol)

[f] The alcohols were synthesized according to Ref. [55]

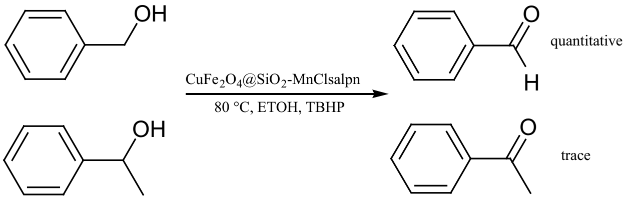

Scheme 3 Chemoselectivity of the catalyst

over homogeneous catalysts. The recovered nanocatalyst was therefore reused for the oxidation of benzyl alcohol, with the results presented in Table 1. The catalytic activity showed only a small reduction for three consecutive uses of the catalyst. We conclude that the manganese species are strongly bonded to the surface of the nanoparticles, such that the nanocatalyst is stable under the reaction conditions and the oxidation is truly heterogeneous. Also, the magnetic properties of the recovered nanocatalyst were investigated after the second recovery, by means of VSM analysis. The saturation magnetization of the recovered nanocatalyst is about 17.5 emu/g, hence there is negligible change in its magnetic properties (see Supplementary Materials Fig. S1). The FTIR spectrum of the reused catalyst also showed no detectable changes compared to the fresh catalyst (see Supplementary Materials Fig. S2).

Table 3 compares the catalyst used in the present study with some other catalysts used for oxidation of benzyl alcohol, as reported in the literature. It can be observed that the catalyst employed here is comparable to, or even superior to, other examples as previously reported.

Conclusions

In this study, a magnetically recoverable nanocatalyst with high thermal stability (> 200 °C) was synthesized from a manganese Schiff base complex anchored on functionalized

Table 3 Comparison of this work with systems described in the literature for the oxidation of benzyl alcohol

Catalyst	Oxidant	Reaction time (h)	Temperature (°C)	Solvent	References
Mn@MNP	TBHP	4	110	DMSO	[56]
SBA-15-pr-NH_2-Mn(Salen)	TBHP	8	90	Acetonitrile	[52]
Mn(salen)Cl-cellulose	Oxone	0.5	25	Ethanol	[57]
Mn(II)2,2-bipyridine complexes/HMS[a]	TBHP	8	90	Acetonitrile	[58]
$[Mn(bpy)_2]^{2+}$/HMS	TBHP	8	90	Acetonitrile	[59]
$CuFe_2O_4@SiO_2$–MnClsalpn	TBHP	1	80	Ethanol	This work

[a] Hexagonal molecular sieves

silica-coated magnetic nanoparticles. The oxidations of alcohols to the related aldehydes or ketones with good-to-excellent yields were efficiently mediated by this material. This system is both cost-effective and environmentally benign, and the catalyst can be readily separated from the reaction mixture and reused.

Acknowledgements The support of this work by Vali-e-Asr University of Rafsanjan is acknowledged.

References

1. Shambayati S, Schreiber S, Trost B, Fleming I (1991) In: Trost BM (ed) Comprehensive organic synthesis. Pargamon Press, New York
2. Sheldon R (2012) Metal-catalyzed oxidations of organic compounds: mechanistic principles and synthetic methodology including biochemical processes. Elsevier, Amsterdam
3. Carey JS, Laffan D, Thomson C, Williams MT (2006) Analysis of the reactions used for the preparation of drug candidate molecules. Org Biomol Chem 4(12):2337–2347
4. Dugger RW, Ragan JA, Ripin DHB (2005) Survey of GMP bulk reactions run in a research facility between 1985 and 2002. Org Process Res Dev 9(3):253–258
5. Arends IW, Sheldon RA (2011) Modern oxidation of alcohols using environmentally benign oxidants. ChemInform 42(44)
6. Sheldon RA, Arends I, Dijksman A (2000) New developments in catalytic alcohol oxidations for fine chemicals synthesis. Catal Today 57(1):157–166
7. Sheldon RA, Arends IW, ten Brink G-J, Dijksman A (2002) Green, catalytic oxidations of alcohols. Acc Chem Res 35(9):774–781
8. Amato ME, Ballistreri FP, Pappalardo A, Tomaselli GA, Toscano RM, Williams DJ (2005) Novel chiral (Salen) MnIII complexes containing a Calix [4] arene unit as catalysts for enantioselective epoxidation reactions of (Z)-aryl alkenes. Eur J Org Chem 16:3562–3570
9. Moghadam M, Tangestaninejad S, Mirkhani V, Mohammadpoor-Baltork I, Mirjafari A, Mirbagheri NS (2010) Multi-wall carbon nanotubes supported molybdenum hexacarbonyl: an efficient and highly reusable catalyst for epoxidation of alkenes with tert-butyl hydroperoxide. J Mol Catal A Chem 329(1):44–49
10. Ulmann PA, Braunschweig AB, Lee O-S, Wiester MJ, Schatz GC, Mirkin CA (2009) Inversion of product selectivity in an enzyme-inspired metallosupramolecular tweezer catalyzed epoxidation reaction. Chem Commun 34:5121–5123
11. Wei S, Tang Y, Xu X, Xu G, Yu Y, Sun Y, Zheng Y (2011) A new heterogeneous chiral (salen) manganese(III) system for enantioselective epoxidation of non-functionalized olefins. Appl Organomet Chem 25(2):146–153
12. Yang JY, Liu SY, Korendovych IV, Rybak-Akimova EV, Nocera DG (2008) Hangman salen platforms containing dibenzofuran scaffolds. Chemsuschem 1(11):941–949
13. Yu K, Lou L-L, Ding F, Wang S, Wang Z, Liu S (2006) Highly enantioselective epoxidation of olefins by Mn(III) salen complex immobilized on MCM-48. Catal Commun 7(3):170–172
14. Kureshy RI, Ahmad I, Noor-ul HK, Abdi SH, Pathak K, Jasra RV (2005) Encapsulation of a chiral Mn III (salen) complex in ordered mesoporous silicas: an approach towards heterogenizing asymmetric epoxidation catalysts for non-functionalized alkenes. Tetrahedron Asymmetry 16(21):3562–3569
15. Kureshy RI, Ahmad I, Noor-ul HK, Abdi SH, Pathak K, Jasra RV (2006) Chiral Mn(III) salen complexes covalently bonded on modified MCM-41 and SBA-15 as efficient catalysts for enantioselective epoxidation of nonfunctionalized alkenes. J Catal 238(1):134–141
16. Ma L, Su F, Zhang X, Song D, Guo Y, Hu J (2014) Epoxidation of alkenes catalyzed by highly ordered mesoporous manganese–salen-based hybrid catalysts. Microporous Mesoporous Mater 184:37–46
17. Zhang H, Wang YM, Zhang L, Gerritsen G, Abbenhuis HC, van Santen RA, Li C (2008) Enantioselective epoxidation of β-methylstyrene catalyzed by immobilized Mn (salen) catalysts in different mesoporous silica supports. J Catal 256(2):226–236
18. Zhang H, Zhang Y, Li C (2006) Enantioselective epoxidation of unfunctionalized olefins catalyzed by the Mn (salen) catalysts immobilized in the nanopores of mesoporous materials. J Catal 238(2):369–381
19. Gong B, Fu X, Chen J, Li Y, Zou X, Tu X, Ding P, Ma L (2009) Synthesis of a new type of immobilized chiral salen Mn(III) complex as effective catalysts for asymmetric epoxidation of unfunctionalized olefins. J Catal 262(1):9–17
20. Tang X, Tang Y, Xu G, Wei S, Sun Y (2008) Highly enantioselective epoxidation of styrene and α-methylstyrene catalyzed by new doubly-immobilized chiral (salen) Mn(III) catalysts. Catal Commun 10(3):317–320
21. Silva AR, Freire C, de Castro B (2004) Jacobsen catalyst anchored onto an activated carbon as an enantioselective heterogeneous catalyst for the epoxidation of alkenes. Carbon 42(14):3027–3030
22. Tu X, Fu X, Hu X, Li Y (2010) Chiral salen Mn(III) immobilized on sulfoalkyl modified ZSP-IPPA as an effective catalyst for asymmetric epoxidation of unfunctionalized olefins. Inorg Chem Commun 13(3):404–407
23. Silva AR, Budarin V, Clark JH, Freire C, De Castro B (2007) Organo-functionalized activated carbons as supports for the covalent attachment of a chiral manganese(III) salen complex. Carbon 45(10):1951–1964
24. Chomoucka J, Drbohlavova J, Huska D, Adam V, Kizek R, Hubalek J (2010) Magnetic nanoparticles and targeted drug delivering. Pharmacol Res 62(2):144–149
25. Laurent S, Dutz S, Häfeli UO, Mahmoudi M (2011) Magnetic fluid hyperthermia: focus on superparamagnetic iron oxide nanoparticles. Adv Coll Interface Sci 166(1):8–23
26. Mahmoudi M, Sant S, Wang B, Laurent S, Sen T (2011) Superparamagnetic iron oxide nanoparticles (SPIONs): development, surface modification and applications in chemotherapy. Adv Drug Deliv Rev 63(1):24–46
27. Sun C, Lee JS, Zhang M (2008) Magnetic nanoparticles in MR imaging and drug delivery. Adv Drug Deliv Rev 60(11):1252–1265
28. Veiseh O, Gunn JW, Zhang M (2010) Design and fabrication of magnetic nanoparticles for targeted drug delivery and imaging. Adv Drug Deliv Rev 62(3):284–304
29. Zhao X, Bao XY, Guo W, Lee FY (2006) Immobilizing catalysts on porous materials. Mater Today 9(3):32–39
30. McCarthy JR, Weissleder R (2008) Multifunctional magnetic nanoparticles for targeted imaging and therapy. Adv Drug Deliv Rev 60(11):1241–1251
31. Shokouhimehr M, Piao Y, Kim J, Jang Y, Hyeon T (2007) A magnetically recyclable nanocomposite catalyst for olefin epoxidation. Angew Chem Int Ed 46(37):7039–7043
32. Saeednia S, Ardakani MH, Parizi ZP, Hafshejani MT (2016) Synthesis and characterization of a magnetically recoverable molybdenum(VI) nanocatalyst for eco-friendly oxidation of alcohols. Transit Met Chem 41(7):767–774
33. Garza-Navarro M, González-González V, Torres-Castro A, Hinojosa M, García-Loera A, José-Yacamán M (2010) Elaboration of

superparamagnetic cobalt–ferrite nanocomposites from films of chitosan chelates. J Appl Polym Sci 117(2):785–792

34. Hu C, Gao Z, Yang X (2008) One-pot low temperature synthesis of MFe_2O_4 (M = Co, Ni, Zn) superparamagnetic nanocrystals. J Magn Magn Mater 320(8):L70–L73
35. Gadkari AB, Shinde TJ, Vasambekar PN (2011) Ferrite gas sensors. IEEE Sens J 11(4):849–861
36. Pershina A, Sazonov A, Ogorodova L (2010) Evaluation of the resistance of DNA immobilized on ferrimagnetic particles of cobalt ferrite nanopowder against nuclease cleavage. Bull Exp Biol Med 149(1):67–69
37. Esmaeilpour M, Sardarian AR, Javidi J (2012) Schiff base complex of metal ions supported on superparamagnetic $Fe_3O_4@SiO_2$ nanoparticles: an efficient, selective and recyclable catalyst for synthesis of 1,1-diacetates from aldehydes under solvent-free conditions. Appl Catal A 445:359–367
38. Kapilevich L, D'yakova EY, Nosarev A, Zaitseva T, Petlina Z, Ogorodova L, Ageev B, Magaeva A, Itin V, Terekhova AO (2010) Effect of nanodisperse ferrite cobalt ($CoFe_2O_4$) particles on contractile reactions in guinea pigs airways. Bull Exp Biol Med 149(1):70–72
39. Yi DK, Lee SS, Ying JY (2006) Synthesis and applications of magnetic nanocomposite catalysts. Chem Mater 18(10):2459–2461
40. Yoon TJ, Yu KN, Kim E, Kim JS, Kim BG, Yun SH, Sohn BH, Cho MH, Lee JK, Park SB (2006) Specific targeting, cell sorting, and bioimaging with smart magnetic silica core–shell nanomaterials. Small 2(2):209–215
41. Ge Q, Huang Y, Qiu F, Li S (1998) Bifunctional catalysts for conversion of synthesis gas to dimethyl ether. Appl Catal A 167(1):23–30
42. Bagherzadeh M, Mortazavi-Manesh A (2015) Immobilized manganese porphyrin on functionalized magnetic nanoparticles via axial ligation: efficient and recyclable nanocatalyst for oxidation reactions. J Coord Chem 68(13):2347–2360
43. Esmaeilpour M, Javidi J, Dodeji FN, Abarghoui MM (2014) M (II) Schiff base complexes (M = zinc, manganese, cadmium, cobalt, copper, nickel, iron, and palladium) supported on superparamagnetic $Fe_3O_4@SiO_2$ nanoparticles: synthesis, characterization and catalytic activity for Sonogashira-Hagihara coupling reactions. Transit Met Chem 39(7):797–809
44. Sun W, Wang H, Xia C, Li J, Zhao P (2003) Chiral-Mn (Salen)-complex-catalyzed kinetic resolution of secondary alcohols in water. Angew Chem Int Ed 42(9):1042–1044
45. Dandia A, Jain AK, Sharma S (2013) $CuFe_2O_4$ nanoparticles as a highly efficient and magnetically recoverable catalyst for the synthesis of medicinally privileged spiropyrimidine scaffolds. RSC Adv 3(9):2924–2934
46. Sobhani S, Pakdin-Parizi Z (2014) Lanthanum(III) triflate supported on nanomagnetic γ-Fe_2O_3: a new magnetically recyclable heterogeneous Lewis acid for the one-pot synthesis of β-phosphonomalonates. RSC Adv 4(25):13071–13077
47. Masteri-Farahani M, Tayyebi N (2011) A new magnetically recoverable nanocatalyst for epoxidation of olefins. J Mol Catal A Chem 348(1):83–87
48. Coleman W, Taylor L (1971) Pentadentate ligands. I. Nickel(II) complexes of the linear Schiff base ligands derived from substituted salicylaldehydes and diethylenetriamine and 2,2′-bis (aminopropyl) amine. Inorg Chem 10(10):2195–2199
49. Jia M, Thiel WR (2002) Oxodiperoxo molybdenum modified mesoporous MCM-41 materials for the catalytic epoxidation of cyclooctene. Chem Commun 20:2392–2393
50. Mukhopadhyay R, Bhattacharjee S, Bhattacharyya R (1994) Ligand control on the synthesis and redox potency of mononuclear manganese-(III) and-(IV) complexes with tridentate ONS co-ordination. J Chem Soc Dalton Trans 19:2799–2804
51. Panella B, Vargas A, Baiker A (2009) Magnetically separable Pt catalyst for asymmetric hydrogenation. J Catal 261(1):88–93
52. Mahdavi V, Mardani M (2015) Mn (Salen) Cl complexes immobilized on SBA-15 functionalized with amine as an efficient, selective and recyclable catalyst for benzyl alcohol oxidation by TBHP: the effects of Mn loading and reaction conditions. Res Chem Intermed 41(11):8907–8927
53. Oh NY, Suh Y, Park MJ, Seo MS, Kim J, Nam W (2005) Mechanistic insight into alcohol oxidation by high-valent iron–oxo complexes of heme and nonheme ligands. Angew Chem 117(27):4307–4311
54. Rahimi R, Ghoreishi SZ, Dekamin MG (2012) Immobilized metalloporphyrins on 3-aminopropyl-functionalized silica support as heterogeneous catalysts for selective oxidation of primary and secondary alcohols. Monatshefte für Chemie-Chem Mon 143(7):1031–1038
55. Mavis ME, Yolacan C, Aydogan F (2010) An investigation of the catalytic potential of mono-and dicationic imidazolium N-heterocyclic carbenes in the benzoin condensation. Tetrahedron Lett 51(34):4509–4511
56. Zhou Q, Wan Z, Yuan X, Luo J (2016) A new magnetic nanoparticle-supported Schiff base complex of manganese: an efficient and recyclable catalyst for selective oxidation of alcohols. Appl Organomet Chem 30(4):215–220
57. Nasseri MA, Mohammadinezhad A, Salimi M (2015) A cellulose-supported Mn (salen) Cl complex as an efficient heterogeneous catalyst for the selective oxidation of benzylic alcohols. J Iran Chem Soc 12(1):81–86
58. Mahdavi V, Mardani M (2012) Selective oxidation of benzyl alcohol with tert-butylhydroperoxide catalysed via Mn(II) 2,2-bipyridine complexes immobilized over the mesoporous hexagonal molecular sieves (HMS). J Chem Sci 124(5):1107–1115
59. Mahdavi V, Mardani M, Malekhosseini M (2008) Oxidation of alcohols with tert-butylhydroperoxide catalyzed by Mn(II) complexes immobilized in the pore channels of mesoporous hexagonal molecular sieves (HMS). Catal Commun 9(13):2201–2204